e^+e^- hadronic cross-sections with SND detector at VEPP 2000

T.V.Dimova[1,2 ⋆], M.N.Achasov[1,2], A.Yu.Barnyakov[1], K.I.Beloborodov[1,2], A.V.Berdyugin[1,2], A.G.Bogdanchikov[1], A.A.Botov[1], V.P.Druzhinin[1,2], L.V.Kardapoltsev[1,2], A.G.Kharlamov[1,2], A.A.Korol[1,2], D.P.Kovrizhin[1], A.S.Kupich[1], N.A.Melnikova[1], A.E.Obrazovsky[1], E.V.Pakhtusova[1], K.V.Pugachev[1,2], S.I.Serednyakov[1,2], D.A.Shtol[1], Z.K.Silagadze[1,2], I.K.Surin[1], Yu.V.Usov[1] and V.N.Zabinv[1]

1 Budker Institute of Nuclear Physics, Novosibirsk, 630090, Russia
2 Novosibirsk State University, Novosibirsk, 630090, Russia
* baiert@inp.nsk.su

November 29, 2021

16th International Workshop on Tau Lepton Physics (TAU2021), September 27 – October 1, 2021
doi:10.21468/SciPostPhysProc.?

Abstract

Data with an integrated luminosity of about 370 pb^{-1} have been collected with the SND detector at the VEPP-2000 e^+e^- collider. Here we present recent results on e^+e^- annihilation into hadrons below 2 GeV based on a part of these data. In particular, we discuss measurements of the $e^+e^- \to \pi^+\pi^-$, $e^+e^- \to n\bar{n}$, $e^+e^- \to p\bar{p}$, and $e^+e^- \to \pi^+\pi^-\pi^0\pi^0$ cross sections, and study of the processes $e^+e^- \to \pi^+\pi^-\pi^0$, $e^+e^- \to K^+K^-\pi^0$, $e^+e^- \to \eta\pi^0\gamma$, and $e^+e^- \to \eta\eta\gamma$.

1 Introduction

The SND [1–4] is the general purpose nonmagnetic detector. The main part of the detector is the spherical three-layer electromagnetic calorimeter based on 1640 NaI(Tl) crystals. In the center of the detector tracking system is situated. This system consists of a 9-layer drift chamber with 24 jet cells and a proportional chamber in a common gas volume. The particle identification is provided by dE/dx measurements in the tracking system and by a system of threshold Cherenkov counters with silica aerogel radiator. The muon system is located outside the calorimeter and consists of proportional tubes and scintillation counters.

SND is collecting data at the VEPP-2000 e^+e^- collider [5] since 2010 in the energy range 0.3–2.0 GeV. A data sample with integrated luminosity of about 370^{-1}pb has been collected. The distribution of integrated luminosity collected by SND over different center-of-mass energy (E_{cm}) regions is presented in Table 1.

Table 1: The distribution of the integrated luminosity recorded by SND at VEPP-2000 over c.m. energy regions.

E_{cm} range (GeV)	0.30–0.97	0.98–1.06	1.06–2.00
luminosity (pb^{-1})	77	31	259

Main physics task of the SND experiment is the study of all possible processes of e^+e^- annihilation into hadrons below 2 GeV. In this energy region the total hadronic cross section is

determined as a sum of cross sections of all processes. Knowledge of the total hadronic cross section with high accuracy is required to evaluate the hadronic contribution to the anomalous magnetic moment of the muon and the fine structure constant. A detailed study of dynamic of exclusive processes is also performed.

2 Process $e^+e^- \to \pi^+\pi^-$

The $e^+e^- \to \pi^+\pi^-$ cross section in the energy region below 1 GeV gives the dominant contribution to the anomalous magnetic moment of the muon. There are many measurements of this process, some of them have systematic uncertainty less than 1%. Our measurement [6] is based on data sample collected in the E_{cm} range 0.53–0.88 GeV, and corresponding to 4.6 pb^{-1} of integrated luminosity which is about 10% of the full SND data set in this range. The three layer structure of SND calorimeter permits to provide e/π separation parameter for event selection [7]. The distribution over separation parameter based on the machine learning approach is shown in Fig. 1(left). The measured $e^+e^- \to \pi^+\pi^-$ cross section is shown in Fig. 1 (right). The fit to the cross section was performed by VMD model with $\rho(770)$, $\omega(782)$ and $\rho(1450)$ resonances. Study of systematic uncertainties is very import part of the analysis. Various contributions to systematic error are shown in Table 2. The contribution to the muon

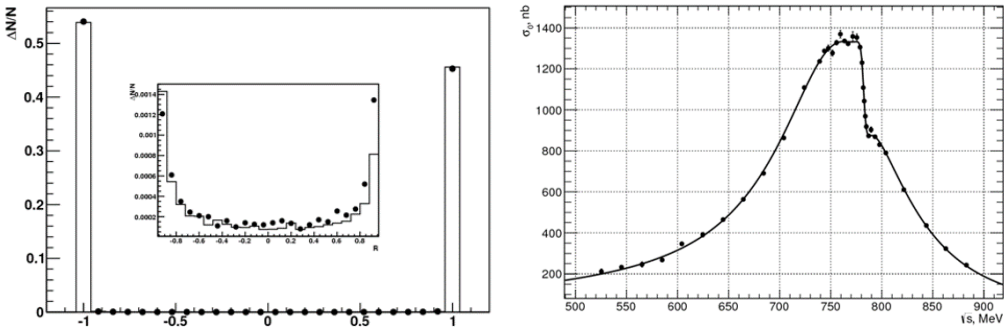

Figure 1: **Left:** The distribution of the e/π separation parameter based on the machine learning approach. **Right:** The $e^+e^- \to \pi^+\pi^-$ cross section measured by SND [6]. The curve is the result of the fit with the VMD model.

Table 2: The systematic uncertainties in the $e^+e^- \to \pi^+\pi^-$ cross section

Source	<0.6 GeV	0.6–0.9 GeV
Trigger(%)	0.5	0.5
Selection criteria(%)	0.6	0.6
e/π (%)	0.5	0.1
Nuclear interaction (%)	0.2	0.2
Theory (%)	0.2	0.2
Total (%)	0.9	0.8

anomalous magnetic moment from the $e^+e^- \to \pi^+\pi^-$ channel in the energy region 0.53–0.88 GeV calculated using the new SND data is $(409.8 \pm 1.4 \pm 3.9) \times 10^{-10}$. This value is in good agreement with the values obtained using the previous SND [8], BABAR [9], and KLOE [10] results.

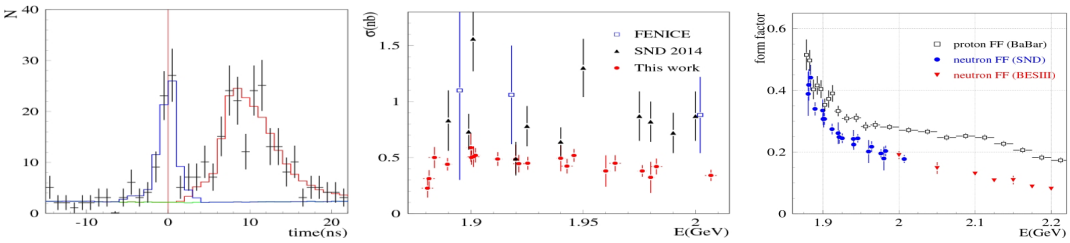

Figure 2: **Left:** The time distribution for selected data events collected in 2019 at $E_{cm} = 1.89$ GeV. The blue histogram is the fitted total contribution of the cosmic-ray, beam-induced and physical backgrounds. The red histogram is the sum of the cosmic-ray background and fitted $n\bar{n}$ signal. **Middle:** The preliminary SND results on the $e^+e^- \to n\bar{n}$ cross section compared with the previous FENICE [11] and SND [12] measurements. Only statistical errors are shown. **Right:** The SND preliminary result on the neutron effective form factor compared with the BESIII [14] neutron form factor and the proton form factor measured by BABAR [15].

.

3 Process $e^+e^- \to n\bar{n}$

The process $e^+e^- \to n\bar{n}$ was previously measured by FENICE [11], and SND [12] using the 2011-2012 data set. The new SND measurement is based on data set collected during 2017 and 2019 years and corresponding to 38 pb^{-1}. A different technique of signal-background separation compared with [12] is used.

For 2017 data, we analyze the distribution of the time difference between the calorimeter trigger and the beam revolution frequency. This difference is measured with a rather poor resolution of about 6 ns. In the 2019 run, due to new electronics the time measurement technique in the calorimeter was significantly improved [13]. So the time resolution measured using $e^+e^- \to \gamma\gamma$ events is 0.8 ns, nearly an order of magnitude lower than that for the 2017 run.

The time distributions for selected data events of the 2019 run at $E_{cm} = 1.89$ GeV are shown in Fig. 2(left). The time distribution consists of the distribution for the beam-induced and physical backgrounds, which is peaked near zero, cosmic-ray distribution, which is nearly uniform, and a wide $n\bar{n}$ distribution, which is shifted relative to other e^+e^- annihilation events due to small anti-neutron velocity. The shape of the beam-induced and physical background distribution is measured using data recorded below the $n\bar{n}$ threshold. From the fit to data with the sum of the three distributions, we determine the number of $n\bar{n}$ events.

Our preliminary result on the $e^+e^- \to n\bar{n}$ cross section is shown in Fig. 2 (middle). The statistical accuracy of the measurement is significantly improved compared with the previous SND measurement [12]. However the new SND result is lower than the previous one. The main reasons are underestimated beam background and not quite correct MC simulation in the previous measurement. The systematic uncertainty on the cross section is estimated to be about 15%, mainly due to MC simulation.

From the measured cross section we determine the effective neutron form factor shown in Fig. 2(right) in comparison with the BESIII measurement of the neutron form factor [14] above 2 GeV and the BABAR measurement of the proton form factor [15]. It is seen that the SND and BESIII results near 2 GeV are in agreement. The proton and neutron effective form factors are close to each other in the near-threshold region. The difference between them grows with increase of the energy.

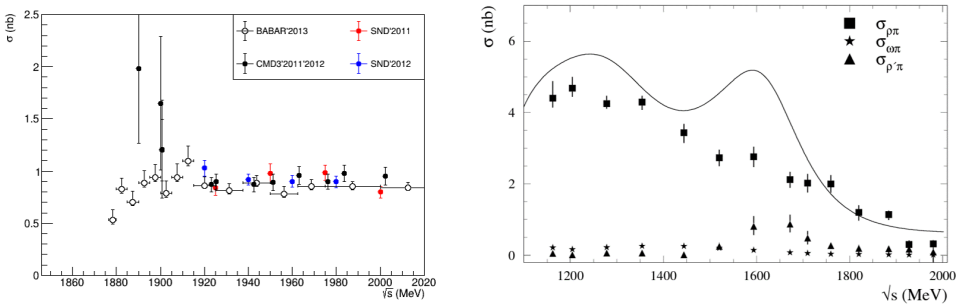

Figure 3: **Left:** The preliminary SND cross section for the $e^+e^- \to p\bar{p}$ process in comparison with the BABAR [15] and CMD-3 [16] results. **Right:** The measured energy dependencies of the cross sections for the intermediate states $\rho(770)\pi$, $\rho(1450)\pi$, and $\omega\pi^0$ [17]. The curve is the result of the VMD fit to the SND data on the total $e^+e^- \to \pi^+\pi^-\pi^0$ cross section.

4 Process $e^+e^- \to p\bar{p}$

The process $e^+e^- \to p\bar{p}$ in the near-threshold region was previously measured by BABAR [15] and CMD-3 [16]. Our measurement is based on 2011 and 2012 data. The analysis is performed in the energy range $E_{cm} > 1.91$ GeV, where protons can penetrate through the drift chamber inner shell and produce tracks. The selection of protons is based on the dE/dx measurement in the drift chamber.

The preliminary results on the $e^+e^- \to p\bar{p}$ cross section obtained separately for 2011 and 2012 data are shown in Fig. 3 (left) in comparison with BABAR [15] and CMD-3 [16] results. Our results are in good agreement with the previous measurements.

5 Process $e^+e^- \to \pi^+\pi^-\pi^0$

Study of dynamics of $e^+e^- \to \pi^+\pi^-\pi^0$ process in the energy range 1.15–2.0 GeV using 2011-2012 data is performed [17]. The Dalitz plot distribution and the $\pi^+\pi^-$ invariant mass spectrum are fitted simultaneously by the model containing the three intermediate states $\rho(770)\pi$, $\rho(1450)\pi$, and $\omega(782)\pi^0$. The result of the fit is shown in Fig. 3(right). The obtained cross sections for each intermediate state are shown together with the total $e^+e^- \to \pi^+\pi^-\pi^0$ cross section.

6 Process $e^+e^- \to K^+K^-\pi^0$

The process $e^+e^- \to K^+K^-\pi^0$ is studied using data set collected during 2011-2012 years. Below 2 GeV this process proceeds mainly through the $K^*(892)^\pm K^\mp$ intermediate state, but the signal from the $\phi\pi^0$ state is also seen. The cross sections for the process $e^+e^- \to K^+K^-\pi^0$ (without $\phi\pi^0$) and $e^+e^- \to \phi\pi^0 \to K^+K^-\pi^0$ have been measured separately [18]. The measured cross sections are shown in Fig. 4 and agree with the previous BABAR measurements [19, 20]. In the narrow region near $\sqrt{s} = 1.58$ GeV all three existing measurements of the $e^+e^- \to \phi\pi^0$ cross section [Fig. 4(right)] show excess over the fit based on the model with $\rho(1450)$ and $\rho(1700)$ vector resonances. Being fitted by the model with $\rho(1700)$ vector resonance and a resonance with free parameters, the following parameters for the narrow

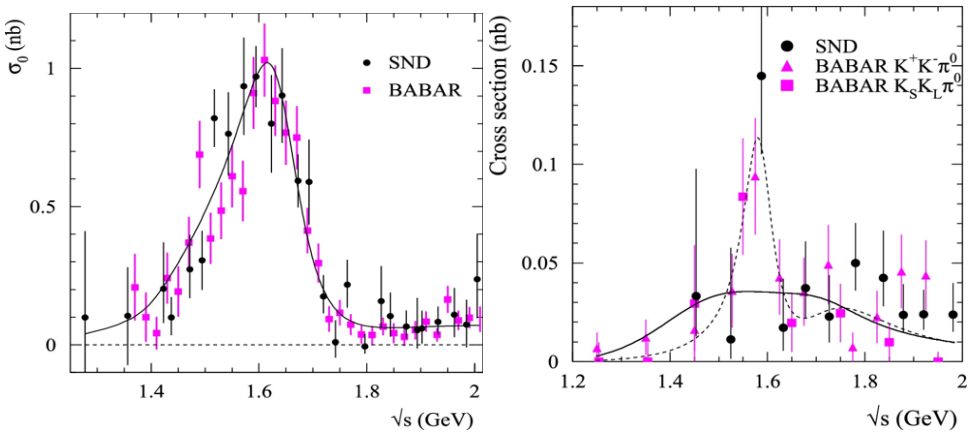

Figure 4: **Left:** The $e^+e^- \to K^+K^-\pi^0$ cross section measured by SND [18] compared with the BABAR [19] data. The curve is the result of the VMD fit with the $\phi(1020)$ and $\phi(1680)$ resonances. **Right:** The $e^+e^- \to \phi\pi^0 \to K^+K^-\pi^0$ cross section measured by SND [18] in comparison with the two BABAR measurements [19,20]. The solid curve represents the VMD fit to the SND and BABAR data with the $\rho(1450)$ and $\rho(1700)$ resonances, while the dashed curves is the result of the fit by a sum of $\rho(1700)$ and a resonance with free parameters.

resonance are obained: $M = 1585 \pm 15$ MeV, $\Gamma = 75 \pm 30$ MeV. Its significance is estimated to be about 3σ.

7 Process $e^+e^- \to \eta\pi^0\gamma$

The process $e^+e^- \to \eta\pi^0\gamma$ above 1.05 GeV is measured for the first time [21]. For the analysis the data set collected during 2010–2012 and 2017 years and corresponding to about 100 pb^{-1} of integrated luminosity is used. Five-photon final state is studied. In this process, there is significant contribution of the $\omega\eta$ intermediate state. But the non-$\omega\eta$ signal is also observed. The significance of non-$\omega\eta$ signal is about 5.6 σ. It may originate from the radiative processes $e^+e^- \to a_0(1450)\gamma$ and $a_2(1320)\gamma$. Figure 5 (left) shows the measured $e^+e^- \to \omega\eta$ cross section in comparison with the SND [22] and CMD-3 [23] measurements in the decay mode $\omega \to 3\pi$. These results are in good agreement. The non-$\omega\eta$ part of the $e^+e^- \to \eta\pi^0\gamma$ cross section is shown in Fig. 5 (right).

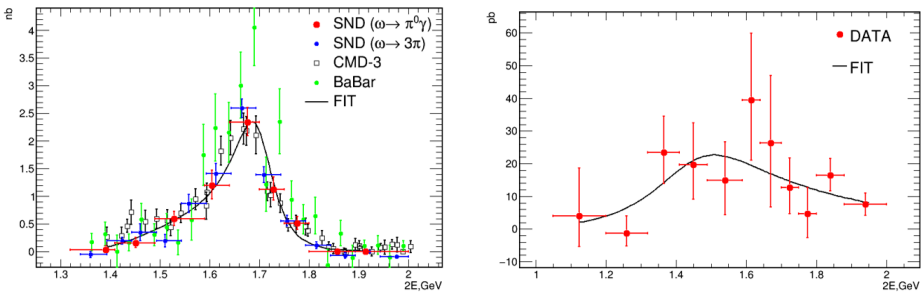

Figure 5: **Left:** The $e^+e^- \to \omega\eta$ cross section measured by SND [21] in the $\eta\pi^0\gamma$ final state in comparison with the SND [22] and CMD-3 [23] measurements in the $\pi^+\pi^-\pi^0\eta$ final state. **Right:** The non-$\omega\eta$ $e^+e^- \to \eta\pi^0\gamma$ cross section measured by SND [21]. The significance of the signal is about 5.6 σ

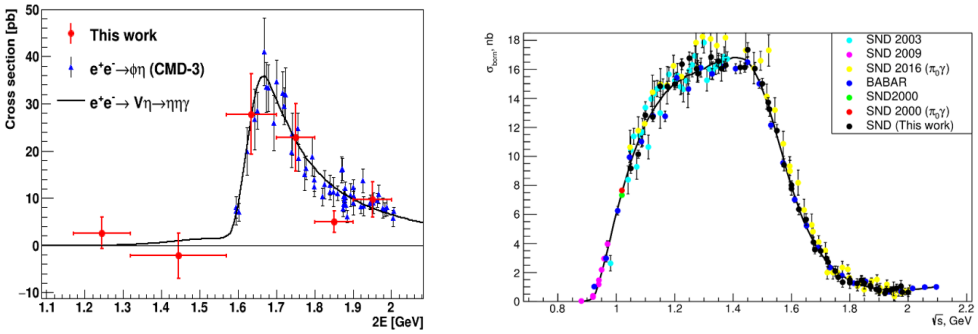

Figure 6: **Left:** The $e^+e^- \to \eta\eta\gamma$ cross section measured by SND [18] compared with the $e^+e^- \to \phi\eta$ cross section measured by CMD-3 in the decay mode $\phi \to K^+K^-$ [25]. The solid curve is the sum of the $e^+e^- \to \phi\eta$, $\rho\eta$, and $\omega\eta$ cross sections. **Right:** The preliminary $e^+e^- \to \omega\pi^0 \to \pi^+\pi^-\pi^0\pi^0$ cross section in comparison with previous SND [26–29] and BABAR [30] results. Solid curve is the fit to the cross section with the VMD model.

8 Process $e^+e^- \to \eta\eta\gamma$

The process $e^+e^- \to \eta\eta\gamma$ above 1.17 GeV is measured for the first time [24]. The analysis is based on data set corresponding to 201 pb^{-1} of integrated luminosity. The final state with five photons is considered. The main intermediate state is $\phi\eta$. The preliminary cross section is shown in Fig. 6(left). The result is consistent with CMD-3 result in $\phi \to K^+K^-$ decay mode [25]. No contribution from other intermediate states is found.

9 Process $e^+e^- \to \omega\pi^0 \to \pi^+\pi^-\pi^0\pi^0$

The process $e^+e^- \to \omega\pi^0 \to \pi^+\pi^-\pi^0\pi^0$ is studied basing on the 35 pb^{-1} data set collected in 2011-2012. This is the first step in the study of $e^+e^- \to \pi^+\pi^-\pi^0\pi^0$ reaction with all possible intermediate states. The $\omega\pi^0$ intermediate state was separated using the fit to the $\pi^+\pi^-\pi^0$ invariant mass ($M_{3\pi}$) spectrum in the 0.6–0.9 GeV range. The restriction $M_{3\pi} < 0.9$ GeV is used to avoid the dependence on the ω shape model. The preliminary cross section shown in Fig. 6(right) is in good agreement with previous measurements [26–30] and have better accuracy. The cross-section data are fitted with the VMD model with three ρ-like resonances.

10 Conclusion

During 2010-2021 the SND detector accumulated data with an integrated luminosity of about 370 pb^{-1} in the E_{cm} range 0.3–2 GeV. Data analysis of various hadron production reactions is in progress.

Acknowledgments

This work is supported in part by the RFBR grants 20-02-00060-a and 20-02-00347.

References

[1] M. N. Achasov *et al.*, Nucl. Instrum. Methods Phys. Res., Sect. A **598** 31 (2009). doi:10.1016/j.nima.2008.08.012

[2] V. M. Aulchenko *et al.*, Nucl. Instrum. Methods Phys. Res., Sect. A **598** 102 (2009). doi:10.1016/j.nima.2008.08.099

[3] A. Y. Barnyakov *et al.*, JINST **9**, C09023 (2014). doi:10.1088/1748-0221/9/09/C09023

[4] V. M. Aulchenko *et al.*, Nucl. Instrum. Methods Phys. Res., Sect. A **598** 340 (2009). doi:10.1016/j.nima.2008.08.127

[5] A. Romanov *et al.*, in *Proceedings of Particle Accelerator Conference PAC 2013, Pasadena, CA USA*, p.14 (2013)

[6] M. N. Achasov *et al.* (SND Collaboration), JHEP **01**, 113 (2021). doi:10.1007/JHEP01(2021)113

[7] M. N. Achasov and A. S. Kupich, JINST **12**, C06035 (2017). doi:10.1088/1748-0221/12/06/C06035

[8] M. N. Achasov *et al.* (SND Collaboration), J. Exp. Theor. Phys. **103**, 380 (2006). doi:10.1134/S106377610609007X

[9] J. P. Lees *et al.* (BaBar Collaboration), Phys. Rev. D**86**, 032013 (2012). doi:10.1103/PhysRevD.86.032013

[10] A. Anastasi *et al.* (KLOE Collaboration), JHEP **03**, 173 (2018). doi:10.1007/JHEP03(2018)173

[11] A. Antonelli *et al.* (FENICE Collaboration), Nucl. Phys. B**517**, 3 (1998). doi:10.1016/S0550-3213(98)00083-2

[12] M. N. Achasov *et al.* (SND Collaboration), Phys. Rev. D**90**, no. 11, 112007 (2014) doi:10.1103/PhysRevD.90.112007

[13] M. N. Achasov *et al.*, JINST, **10**, T06002 (2015). doi:10.1088/1748-0221/10/06/T06002

[14] M. Ablikim *et al.* (BESIII Collaboration), arXiv:2103.12486 [hep-ex].

[15] J. P. Lees *et al.* (BaBar Collaboration), Phys. Rev. D **87**, 092005 (2013). doi:10.1103/PhysRevD.87.092005

[16] R.R. Akhmetshin *et al.* (CMD-3 Collaboration) Phys. Lett. B**759**, 634 (2016). doi:10.1016/j.physletb.2016.04.048

[17] M. N. Achasov *et al.* (SND Collaboration), Eur. Phys. J. C**80**, 993 (2020). doi:10.1140/epjc/s10052-020-08524-4

[18] M. N. Achasov *et al.* (SND Collaboration), Eur. Phys. J. C**80**, 1139 (2020). doi:10.1140/epjc/s10052-020-08719-9

[19] B. Aubert *et al.* (BABAR Collaboration), Phys. Rev. D**77**, 092002 (2008). doi:10.1103/PhysRevD.77.092002

[20] J. P. Lees *et al.* (BABAR Collaboration), Phys. Rev. D**95**, 052001 (2017). doi:10.1103/PhysRevD.95.052001

[21] M. N. Achasov *et al.* (SND Collaboration), Eur. Phys. J. C**80**, 1008 (2020). doi:10.1140/epjc/s10052-020-08556-w

[22] M. N. Achasov *et al.* (SND Collaboration), Phys. Rev. D**99**, 112004 (2019). doi:10.1103/PhysRevD.99.11200

[23] R. R. Akhmetshin *et al.* (CMD-3 Collaboration), Phys. Lett. B**773**, 150 (2017). doi:10.1016/j.physletb.2017.08.019

[24] M. N. Achasov *et al.* (SND Collaboration), arXiv:2110.05845 [hep-ex].

[25] V. L. Ivanov *et al.* (CMD-3 Collaboration) Phys. Lett. B **798**, 134946 (2019). doi:10.1016/j.physletb.2019.134946

[26] M. N. Achasov *et al.*, Phys. Lett. B**486**, 29 (2000) doi:10.1016/S0370-2693(00)00706-1

[27] M. N. Achasov *et al.*, Phys. Rev. D**94**, 112001 (2016) doi:10.1103/PhysRevD.98.112001

[28] M. N. Achasov *et al.*, J. Exp. Theor. Phys. **96**, 789 (2003) doi:10.1134/1.1581933

[29] M. N. Achasov *et al.*, J. Exp. Theor. Phys. **109**, 379 (2009) doi:10.1134/S1063776109090039

[30] J. P. Lees *et al.* (BaBar Collaboration), Phys. Rev. D**96**, 092009 (2017) doi:10.1103/PhysRevD.96.092009